Poisson Multi-Bernoulli Mixture Filtering with Multistatic Passive Bistatic Radar

Viktor Deleskog*, Oskar Jonsson†, Jonas Nygårds*, and Gustaf Hendeby‡
* Div. of Cyber defence and C2 technology,
† Div. of Electromagnetic Warfare,
Swedish Defence Research Agency (FOI), Linköping, Sweden
e-mail: firstname.lastname@foi.se
‡ Dept. of Electrical Engineering, Linköping University, Linköping, Sweden
e-mail: gustaf.hendeby@liu.se

***Abstract*—Passive bistatic radar (PBR) is a cost-effective choice for detection and tracking of aircraft. In this paper we present how the Poisson multi-Bernoulli mixture (PMBM) filter is applied in a multi-target tracking application with multistatic PBR. To handle the PBR measurements, it is proposed that a Gaussian mixture target spatial density is used to represent the target state. A state dependent probability of detection model for PBR is presented and how it is used to design the target birth model. Simulated and experimental data are used to evaluate the performance of the described approaches.**

***Index Terms*—Poisson multi-Bernoulli mixture filter, multi-target tracking, passive bistatic radar**

I. Introduction

Mostly, air surveillance for air traffic control (ATC) relies on all aircraft actively sending ego-information (such as identity, position, speed, and heading) using a transponder, *e.g.* automatic dependent surveillance-broadcast (ADS-B). This data is used by the ATC to generate a real-time air situational picture. In situations when an aircraft is not equipped with a transponder (*e.g.* military aircraft) or its transponder malfunctions or even is actively turned off, the ATC cannot detect the aircraft. Then, a primary radar is required. A more cost effective option is passive bistatic radar (PBR), since there is no need for an active transmitter [6].

In PBR, illuminators of opportunity, *e.g.* TV (DVB-T), radio (FM), and base stations for mobile phones, are exploited as target illuminators. The system measures the direct signal and the scattered radiation caused by the target. The delay between these signals is interpreted as the bistatic range and the Doppler shift caused by motion is interpreted as the bistatic range rate [2]. The system is radio silent so it is also interesting for covert military applications [4, 6]. In this paper we consider multistatic PBR by exploiting multiple FM radio broadcast (87.5 MHz-108 MHz) transmitters as illuminators of opportunity for passive air surveillance.

To create an aerial situational picture using PBR, a tracking algorithm is required to handle measurements generated from true targets, false targets, and clutter. In [3, 4, 11] a two-stage tracking approach is applied to handle bistatic measurements with FM and DVB-T transmitters. In the first stage, targets are tracked in the bistatic plane (range and range rate). In the second stage, confirmed bistatic tracks are used to initiate Cartesian tracks. In both stages, a multi-hypothesis tracking (MHT) [1] algorithm is used. A particle filtering approach is presented in [8] where the data association is performed by the particle filter. Each target is tracked using a separate particle filter and measurements are associated using the nearest neighbor algorithm. The computational cost of the filter is high so the clutter level is therefore assumed to be zero. Also, the probability hypothesis density (PHD) filter has been used for FM transmitters of opportunity [15] and for Doppler-only measurements in a two-stage approach [14].

Lately, the PMBM filter [17] has gained attention in multiple tracking applications. The filter is based on a Bayesian approach of the complete multi-target tracking problem which in theory is optimal. In [5], a derivation of the PMBM filter is presented together with a proposed implementation for linear and Gaussian models.

In this work we are interested in how to apply the PMBM filter to PBR. The PMBM is a union of two independent processes: a Poisson point process (PPP), for unseen targets, and a multi-Bernoulli mixture (MBM) process, for already observed target. This enables a more flexible way to initiate new targets and has been shown to handle environments with high rates of false measurements [17].

The contribution of this paper is to show how the PMBM filter can be applied to multi-target tracking using a multistatic PBR system. A Gaussian mixture is proposed to represent the target density. Also, an appropriate target birth design for PBR is presented. The results show better tracking performance compared the standard PMBM implementation [5], in both simulated and experimental data.

The paper is organized as follows. In Sec. II, an introduction to PBR is given together with an overview of the PMBM filter. Sec. III presents the modeling of the PBR and how it is integrated within the PMBM filter framework. Sec. III-C describes a proposed approach to integrate PBR measurements with the PMBM filter and Sec. III-B presents a tailored birth process design. Sec. IV presents the experimental results using the proposed approaches in simulated and real scenarios. Sec. V concludes the paper.

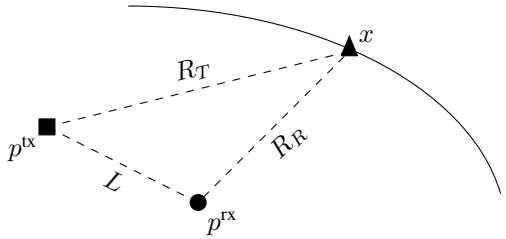

Fig. 1: Illustration of the passive bistatic radar geometry defined by a receiver at p^{rx}, a transmitter at p^{tx}, and a target x. A part of the iso-range ellipse that corresponds to the bistatic range is illustrated as a solid line.

II. Background

This section presents the key parts of PBR and the PMBM filter.

A. Passive bistatic radar

A PBR is a combination of one or multiple bistatic pairs, where a bistatic pair is formed by one transmitter and one receiver, separated from each other. The bistatic range R is measured as the time delay between the target reflected signal and the direct signal. From the geometry in Fig. 1 we compute the bistatic range as

$$R = R_T + R_R - L \ , \tag{1}$$

where R_T is the transmitter-to-target range, R_R is the receiver-to-target range, and L is the baseline between transmitter and receiver. These are computed as

$$\begin{aligned} R_T &= \|p - p^{\text{tx}}\| \\ R_R &= \|p - p^{\text{rx}}\| \\ L &= \|p^{\text{tx}} - p^{\text{rx}}\| \end{aligned} \tag{2}$$

where p is the location of the target and p^{rx} and p^{tx} are the locations of the receiver and transmitter, respectively. The bistatic range defines an iso-range ellipse, where the target is located, where the position of the transmitter and receiver are the two focal points, see Fig. 1. Also, due to target motion, the bistatic range rate is measured via the observed Doppler shift of the reflected signal. From the geometry, the bistatic range rate is computed as

$$\dot{R} = \dot{R}_T + \dot{R}_R = \left(\frac{p - p^{\text{tx}}}{R_T} + \frac{p - p^{\text{rx}}}{R_R} \right) \cdot v \tag{3}$$

where $\cdot$ denotes the dot product of two vectors and v is the target velocity.

B. Poisson Multi-Bernoulli Mixture Filter

The PMBM filter is based on random finite set (RFS) theory [9]. In RFS-based filtering, the multi-target state and the measurements are modeled as two RFSs, X and Z, respectively. In the end we want to estimate the posterior of the multi-target state density $\pi_{k|k}(X_k|Z_{1:k})$ at current time step k given all observed measurements up to and including time step k. In the PMBM filter, the set of targets X is divided into two disjoint subsets $X^u \uplus X^d = X$, where X^u contains the undetected targets and X^d contains the observed targets. X^u is modeled by a Poisson point process (PPP), and X^d is modeled by a multi-Bernoulli mixture (MBM). The PMBM is given by

$$\pi^{\text{PMBM}}(X) = \sum_{X^u \uplus X^d = X} \pi^{\text{PPP}}(X^u) \pi^{\text{MBM}}(X^d) \tag{4}$$

where $\pi^{\text{PPP}}(X^u)$ and $\pi^{\text{MBM}}(X^d)$ are the PPP and MBM RFS densities, respectively.

Next, a brief overview of the implementation in [5] for linear and Gaussian models is given. Let the PMBM density in (4) be defined by the parameters

$$\lambda^u, \{w^j, \{r^{j,i}, p^{j,i}\}_{i \in \mathbb{I}^j}\}_{j \in \mathbb{J}} \tag{5}$$

where λ^u is the intensity of undetected targets and $\mathbb{J}$ is an index set for all global hypotheses. The jth multi-Bernoulli (MB) component has weight w^j with density π^j and consists of $|\mathbb{I}^j|$ components. The density of the i:th Bernoulli component under global hypothesis j is defined by the existence probability $r^{j,i}$ and spatial density $p^{j,i}$.

Given the single target state x and associated measurement z, at time step k,

$$\begin{aligned} p(x_k|x_{k-1}) &= \mathcal{N}(x_k; F x_{k-1}, Q) \\ p(z_k|x_k) &= \mathcal{N}(x_k; H x_k, R) \end{aligned} \tag{6}$$

where $p(x_k|x_{k-1})$ is the transition density and $p(z_k|x_k)$ is the measurement likelihood. Also, it is assumed that the probability of detection and the probability of survival are constants, *i.e.* $p_{\text{D}}(x) \equiv p_{\text{D}}$ and $p_S(x) \equiv p_S$.

1) Prediction step: Let the posterior of the Poisson process at the previous time step k be a Gaussian mixture,

$$\lambda^u(x) = \sum_{i=1}^{N_u} w_{k|k}^{u,i} \mathcal{N}(x; \hat{x}_{k|k}^{u,i}, P_{k|k}^{u,i}) \tag{7}$$

and the MBM parameters are $w_{k|k}^{j,i}$, $p^{j,i}(x) = \mathcal{N}(x; \hat{x}_{k|k}^{j,i}, P_{k|k}^{j,i})$, and $r_{k|k}^{j,i}$. The predicted intensity is then found as a Gaussian mixture,

$$\mu(x) = \lambda^b(x) + p_S \sum_{i=1}^{N_u} w_{k|k}^{u,i} \mathcal{N}(x; F\hat{x}_{k|k}^{u,i}, F P_{k|k}^{u,i} F^T + Q) \tag{8}$$

where $\lambda^b(x)$ is the newborn target intensity. The predicted Bernoulli components have the same weights $w_{k+1|k}^{j,i} = w_{k|k}^{j,i}$ with existence probability $r_{k+1|k}^{j,i} = p_S r_{k|k}^{j,i}$ and

$$p_{k+1|k}^{j,i}(x) = \mathcal{N}(x; F\hat{x}_{k|k}^{j,i}, F P_{k|k}^{j,i} F^T + Q) \ . \tag{9}$$

2) Update step: First, the predicted intensity of the Poisson component in (8) is rewritten as

$$\mu(x) = \sum_{i=1}^{N_\mu} w_{k|k-1}^{\mu,i} \mathcal{N}(x; \hat{x}_{k|k-1}^{\mu,i}, P_{k|k-1}^{\mu,i}) \tag{10}$$

which is updated to the current time step k by simply multiplying with $1 - p_{\text{D}}$.

The update of potential targets detected for the first time is as follows. To decrease the computational complexity, ellipsoidal gating is performed on measurements for all components in the Poisson prior. For each measurement z_k that is within the gating limits, generates a new Bernoulli component with parameters

$$r_{k|k} = \frac{C}{\lambda^{\text{FA}}(z_k) + C} \tag{11a}$$

$$p_{k|k}(x) = \sum_{i=1}^{N^\mu} \frac{c_i}{C} \mathcal{N}(x; \hat{x}_{k|k}^{\mu,i}, P_{k|k}^{\mu,i}) \tag{11b}$$

$$w_{k|k} = \lambda^{\text{FA}}(z_k) + C \tag{11c}$$

using standard Kalman update equations, where $\lambda^{\text{FA}}(z_k)$ is the false alarm intensity. The component weights are computed as

$$c_i = p_{\text{D}} w_{k|k-1}^{\mu,i} \mathcal{N}(z_k; H\hat{x}_{k|k-1}^{\mu,i}, S_k^{\mu,i}) \ , \ C = \sum_{i=1}^{N^\mu} c_i \tag{12}$$

where $\mathcal{N}(z_k; H\hat{x}_{k|k-1}^{\mu,i}, S_k^{\mu,i})$ is the measurement likelihood and S denotes the innovation covariance matrix. To reduce the computational complexity, the Gaussian mixture in (11) is approximated as a single Gaussian by moment matching.

Next, consider a predicted Bernoulli component with existence probability $r_{k|k-1}^{j,i}$, state density $p_{k|k-1}^{j,i}(x)$, and mixture weight $w_{k|k-1}^{j,i}$. At time step k, this component generates one misdetection hypothesis and one updated hypothesis for each measurement within the gate. Under the misdetection hypothesis the same density is obtained, but

$$r_{k|k}^{j,i} = \frac{r_{k|k-1}^{j,i}(1 - p_{\text{D}})}{1 - r_{k|k-1}^{j,i} + r_{k|k-1}^{j,i}(1 - p_{\text{D}})} \tag{13a}$$

$$w_{k|k}^{j,i} = w_{k|k-1} \left(1 - r_{k|k-1}^{j,i} + r_{k|k-1}^{j,i}(1 - p_{\text{D}})\right) \ . \tag{13b}$$

Under the hypothesis that the target is associated to measurement z_k, we have

$$r_{k|k}^{j,i} = 1 \tag{14a}$$

$$p_{k|k}^{j,i}(x) = \mathcal{N}(x; \hat{x}_{k|k}^{j,i}, P_{k|k}^{j,i}) \tag{14b}$$

$$w_{k|k}^{j,i} = w_{k|k-1}^{j,i} r_{k|k-1}^{j,i} p_{\text{D}} \mathcal{N}(z_k; H\hat{x}_{k|k-1}^{j,i}, S_k^{j,i}) \tag{14c}$$

using standard Kalman update equations, where the measurement likelihood is $\mathcal{N}(z_k; H\hat{x}_{k|k-1}^{j,i}, S_k^{j,i})$. More details and a complete derivation are found in [5, 17].

III. Filter adaptations for passive bistatic radar

This section presents how PBR measurements can be used by the PMBM filter in a multi-sensor aircraft tracking application. First, we present our PBR sensor model to be used for filtering. It includes the measurement model, the state dependent probability of detection model, and the model for false alarms. Secondly, a target birth model design is presented that exploits properties of the PBR sensor model. Lastly, we revise the standard implementation in Sec. II-B to handle multi-sensor PBR measurements.

A. PBR sensor model

We assume two-dimensional target motion at constant altitude to limit the scope of this paper. This approximation is justified by the low range cell resolution (~ 1000 m) using FM signals.

Measurement model: Let a single target at time step k be represented by the state vector $x_k = [p_k, v_k]^T$, where $p_k = [p_k^x, p_k^y]^T$ is the position vector and $v_k = \left[v_x^k, v_y^k\right]^T$ is the velocity vector in a two-dimensional Cartesian space. Let the receiver be positioned at the origin $x^{\text{rx}} = [0, 0]^T$ and the transmitter at $x^{\text{tx}} = \left[p_x^{\text{tx}}, p_y^{\text{tx}}\right]^T$. Using (1)-(3), the bistatic range $r(x_k, x^{\text{tx}})$ and the bistatic range rate $\dot{r}(x_k, x^{\text{tx}})$ of a target x_k, measured by this bistatic pair are computed as

$$r(x_k, x^{\text{tx}}) = \|p_k - x^{\text{tx}}\| + \|p_k\| - L \tag{15a}$$

$$L = \|x^{\text{tx}} - x^{\text{rx}}\|$$

$$\dot{r}(x_k, x^{\text{tx}}) = \left(\frac{p_k - x^{\text{tx}}}{\|p_k - x^{\text{tx}}\|} + \frac{p_k}{\|p_k\|}\right) \cdot v_k \ . \tag{15b}$$

Denote the measured values of the bistatic range and bistatic range rate at time step k as z^1 and z^2, respectively. The measurement is represented by the vector $z_k = [z^1, z^2]^T$, which is assumed to be Gaussian distributed as

$$l(z_k|x_k) = \mathcal{N}(z_k; h(x_k, x^{\text{tx}}), R_k) \tag{16}$$

where

$$h(x_k, x^{\text{tx}}) = \left[r(x_k, x^{\text{tx}}), \dot{r}(x_k, x^{\text{tx}})\right]^T$$

$$R_k = \begin{bmatrix} \sigma_r^2 & 0 \\ 0 & \sigma_{\dot{r}}^2 \end{bmatrix}$$

using (15), where σ_r and $\sigma_{\dot{r}}$ are the standard deviations of the bistatic range noise and bistatic range rate noise, respectively. The receiver is limited to measuring bistatic ranges in the interval $[r^{\min}, r^{\max}]$ and bistatic range rates in $[\dot{r}^{\min}, \dot{r}^{\max}]$.

Probability of detection: The detection performance of the receiver is limited by the signal-to-noise ratio (SNR). The SNR is computed using the well-known radar range equation [13]. Here, we model the SNR at the receiver of a target with state x_k as

$$\begin{aligned} \text{SNR}(x_k; x^{\text{tx}}, \theta) =& L_D \left(\frac{1}{R_{\text{rx}}(x_k)^2 R_{\text{tx}}(x_k; x^{\text{tx}})^2} \cdot \right. \\ & \left. \frac{1}{L_A(x_k; x^{\text{tx}}, \theta) L_{\text{DSI}}(x_k; x^{\text{tx}})} \right) \\ R_{\text{rx}}(x_k) =& \|p_k\| \\ R_{\text{tx}}(x_k; x^{\text{tx}}) =& \|p_k - x^{\text{tx}}\| \\ L_A(x_k; x^{\text{tx}}, \theta) \in& [0, 1] \\ L_{\text{DSI}}(x_k; x^{\text{tx}}) \in& [0, 1] \end{aligned} \tag{17}$$

where $R_{\text{rx}}(\cdot)$ and $R_{\text{tx}}(\cdot)$ are the distances to target from receiver and transmitter, respectively. $L_A(\cdot)$ and $L_{\text{DSI}}(\cdot)$ are loss terms. Lastly, L_D is used as a design parameter to approximate for the factors of the radar equation that have not been included in this model, *e.g.* bistatic radar cross section (RCS), integration gain, and system losses. Here, it

is computed by assuming a certain SNR at a specific bistatic range. The loss term $L_A(\cdot)$ models the receiver antenna pattern in the horizontal plane, *i.e.* the directional dependence of the antenna gain. In PBR, suppression of direct signal interference (DSI) is used to mitigate the interference effects of the direct signal sensed by the receiver antenna [6]. Here, we model it as an antenna pattern with a notch in the direction of the transmitter.

Further, we assume that target responses fluctuate according to the Swerling 1 case [13]. Given Swerling 1, the probability of detection of a target x_k is expressed as

$$p_{\text{D}}(x_k; x^{\text{tx}}, \theta) = p_{\text{FA}}^{1/(1+\text{SNR}(x_k; x^{\text{tx}}, \theta))} \tag{18}$$

where p_{FA} is the desired probability of false alarms and $\text{SNR}(x_k; x^{\text{tx}}, \theta)$ is given by (17). Given the bistatic range measurement space,

$$p_{\text{D}}(x; x^{\text{tx}}, \theta) = \begin{cases} p_{\text{D}}(x; x^{\text{tx}}, \theta), & r(x, x^{\text{tx}}) \in [r^{\min}, r^{\max}] \\ 0, & \text{otherwise} \end{cases} \tag{19}$$

and $p_{\text{D}}(x; x^{\text{tx}}, \theta) \leq p_{\text{D}}^{\max}$.

False alarms: In addition to true measurements, false measurements are prominent in the receiver. These are modeled as a PPP and are uniformly distributed in the measurement space of the receiver. The intensity function of false measurements is defined as

$$\lambda^{\text{FA}}(z_k) = \bar{\lambda}^{\text{FA}} \cdot \mathcal{U}(z_1; r^{\min}, r^{\max}) \cdot \mathcal{U}(z_2; \dot{r}^{\min}, \dot{r}^{\max}) \tag{20}$$

where $\bar{\lambda}^{\text{FA}}$ is the mean number of false measurements per frame and $\mathcal{U}(\cdot; a, b)$ denotes a uniform density on the interval $[a, b]$. The measurement space is, in fact, divided into cells defined by range and Doppler cell resolution, respectively. If a measurement z_k is in the measurement space we have

$$\lambda^{\text{FA}}(z_k) = \frac{\bar{\lambda}^{\text{FA}}}{n_{\text{range cells}} \cdot n_{\text{Doppler cells}}} \ . \tag{21}$$

B. Target birth

This section describes how the birth process can be designed to handle target birth from PBR measurements. As proposed in [5], let the birth process PPP be a Gaussian mixture with intensity

$$\lambda^b(x) = \sum_{i=1}^{N_b} w^{b,i} \mathcal{N}(x; x^{b,i}, P^{b,i}) \tag{22}$$

consisting of N_b components where $x^{b,i}$ is the mean, $P^{b,i}$ is the covariance and $w^{b,i}$ is the weight of each component. Fig. 1 shows that a measurement from one transmitter only gives information that the target position is on the bistatic range ellipse. Since a single measurement can give birth to a potentially detected target, care must be taken when designing the birth process. Usually, the birth process is designed as a single large Gaussian or a set of multiple Gaussians distributed along the boundary of the surveillance area. Here, we define the surveillance area as the two dimensional region of (x, y) coordinates where the probability of detection, as defined in (18), is greater than or equal the threshold $p_{\text{D}}^{\min}$ in at least $N_S^{\min}$ sensors. This region is computed using grid search, and the birth components in (22) are placed along its boundary. By placing the components on this boundary, we handle both the bistatic geometry and predicted detection performance.

C. Implementation details

Here, we present how to integrate the PBR sensor model into the PMBM filter framework. As a basis we start from the single sensor implementation presented in Sec. II-B and propose required adaptations.

Gaussian mixture state density: In (11), new targets are approximated as a single Gaussians to reduce the computational complexity. However, in PBR, this will give rise to an incorrect initial target density. In Fig. 1 it is shown that a single measurement can be described by a target located anywhere on the bistatic range ellipse. This approximation will return a large Gaussian component with the mean in the center of the associated birth components, see (11b), and a covariance of the same size as the spatial distribution of the birth components.

Probability of detection: To utilize the state dependent probability of detection model in Sec. III-A, we need to address the assumption in the standard implementation that p_{D} is constant. Instead, we approximate that the probability of detection is constant around the center point of the state density. This approximation is motivated by the assumption that $p_{\text{D}}(x)$ varies slowly around the state density [7]. Therefore, p_{D} is replaced with $p_{\text{D}}(x)$.

Nonlinear measurement model: Since the standard implementation assumes linear models, it is required that the update equations are adapted to handle the nonlinear measurement model in (16). We approximate the update equations using standard Extended Kalman Filter (EKF) equations.

Multi-sensor update: The standard implementation of the PMBM filter supports only single sensor update. To implement multi-sensor support, we apply the iterated-corrector approximation presented in [10]. This includes the update of the Poisson component and the MBM component of the filter.

Implementation of adaptations: Next, we summarize how the standard implementation needs to be updated to handle the adaptations above. Let

$$p(z_k|x_k) = \mathcal{N}(z_k; h(x_k), R) \tag{23a}$$

$$p(x) = \sum_{m=1}^{N_m} \eta^m \mathcal{N}(x; \hat{x}^m, P^m) \tag{23b}$$

where $p(z_k|x_k)$ is the nonlinear measurement likelihood and $p(x)$ is a Gaussian mixture state density consisting of N_m components with scalar weights η^m. Also, let

$$\bar{\hat{x}} = \sum_{m=1}^{N_m} \eta^m \hat{x}^m \tag{24}$$

be the mean of (23b).

In the prediction step we only need to revise the prediction of the Bernoulli components in the MBM. The state density $p(x)$ is now a Gaussian mixture, so (9) is replaced with

$$p_{k+1|k}^{j,i}(x) = \sum_{m=1}^{N_m^{j,i}} \eta_{k+1|k}^{j,i,m} \mathcal{N}(x; F\hat{x}_{k|k}^{j,i,m}, FP_{k|k}^{j,i,m}F^T + Q) \tag{25}$$

where $\eta_{k+1|k}^{j,i,m} = \eta_{k|k}^{j,i,m}$.

The predicted intensity of undetected targets in (8) is just updated with the constant $1 - p_{\mathrm{D}}$. Now, the probability of detection is state dependent, so each weight is updated according to

$$w_{k|k}^{\mu,i} = \big(1 - p_{\mathrm{D}}(\hat{x}_{k+1|k}^{u,i})\big) w_{k|k+1}^{\mu,i} \ . \tag{26}$$

Next, we describe the update of new and existing targets respectively. Let the target state density of the new Bernoulli component stay as a Gaussian mixture

$$p_{k|k}(x) = \sum_{i=1}^{N^{\mu}} \frac{c_i}{C} \mathcal{N}(x; \hat{x}_{k|k}^{\mu,i}, P_{k|k}^{\mu,i}) \tag{27}$$

where

$$\begin{aligned} \hat{x}_{k|k}^{\mu,i} &= \hat{x}_{k|k-1}^{\mu,i} + K\left(z_k - h(\hat{x}_{k|k-1}^{\mu,i})\right) \\ c_i &= p_{\mathrm{D}}(\hat{x}_{k|k-1}^{\mu,i}) w_{k|k}^{\mu,i} \mathcal{N}\left(z_k; h(\hat{x}_{k|k-1}^{\mu,i}), S_k^{\mu,i}\right) \\ H &= \left.\frac{\partial h}{\partial x}\right|_{x=\hat{x}_{k|k-1}^{\mu,i}}, \ C = \sum_{i=1}^{N^{\mu}} c_i \end{aligned}$$

and H is the Jacobian of the measurement model evaluated at the state prediction.

For the misdetection hypothesis we have to update the existence probabilities and mixture weights in (13) according to

$$r_{k|k}^{j,i} = \frac{r_{k|k-1}^{j,i}\left(1 - p_{\mathrm{D}}(\bar{\hat{x}}_{k|k-1}^{j,i})\right)}{1 - r_{k|k-1}^{j,i} + r_{k|k-1}^{j,i}\left(1 - p_{\mathrm{D}}(\bar{\hat{x}}_{k|k-1}^{j,i})\right)} \tag{28a}$$

$$\begin{aligned} w_{k|k} = &\, w_{k|k-1} \\ &\cdot \left(1 - r_{k|k-1}^{j,i} + r_{k|k-1}^{j,i}\left(1 - p_{\mathrm{D}}(\bar{\hat{x}}_{k|k-1}^{j,i})\right)\right) \end{aligned} \tag{28b}$$

where $\bar{\hat{x}}_{k|k-1}^{j,i}$ is the mean of the Gaussian mixture state density. Under the hypothesis that the target is detected by a measurement, we update the state density and mixture weight parameters in (14) as

$$p_{k|k}^{j,i}(x) = \sum_{m=1}^{N_m^{j,i}} \eta_{k|k}^{j,i,m} \mathcal{N}(x; \hat{x}_{k|k}^{j,i,m}, P_{k|k}^{j,i,m}) \tag{29a}$$

$$\begin{aligned} w_{k|k}^{j,i} = &\, r_{k|k-1}^{j,i} p_{\mathrm{D}}(\bar{\hat{x}}_{k|k-1}^{j,i}) \\ &\cdot \prod_{m=1}^{N_m} \eta_{k|k-1}^{m} \mathcal{N}(z_k; h(\hat{x}_{k|k-1}^{j,i,m}), S_k^{j,i,m}) \end{aligned} \tag{29b}$$

where

$$\hat{x}_{k|k}^{j,i,m} = \hat{x}_{k|k-1}^{j,i,m} + K(z_k - h(\hat{x}_{k|k-1}^{j,i,m})) \tag{30a}$$

$$P_{k|k}^{j,i,m} = P_{k|k-1}^{j,i,m} - KHP_{k|k-1}^{j,i,m} \tag{30b}$$

$$\eta_{k|k}^{m} = \eta_{k|k-1}^{m} \mathcal{N}(z_k; h(\hat{x}_{k|k-1}^{j,i,m}), S_k^{j,i,m}) \tag{30c}$$

$$K = P_{k|k-1}^{j,i,m} H^T (S_k^{j,i,m})^{-1} \tag{30d}$$

$$S_k^{j,i,m} = HP_{k|k-1}^{j,i,m} H^T + R \tag{30e}$$

and

$$H = \left.\frac{\partial h}{\partial x}\right|_{x=\hat{x}_{k|k-1}^{j,i,m}} . \tag{30f}$$

IV. Experimental results

Here we evaluate how the PMBM filter performs in one simulated and two real scenarios. The proposed Gaussian mixture state density model approach is validated by comparing with the standard approach, where a new target is approximated as a single Gaussian. To evaluate the performance, we apply the generalized optimal sub-pattern assignment (GOSPA) error metric [12] with parameters $p = 2$ (*i.e.* Euclidean distance), cutoff distance $c = 2\,000$ m and $\alpha = 2$. The cutoff distance is motivated by the range resolution and modeling approximations.

Each target survives with the probability $p_S = 0.99$ and moves according to a nearly constant velocity model

$$\begin{aligned} f(x|x') &= \mathcal{N}(x; F_{\mathrm{CV}} x', Q) \\ F_{\mathrm{CV}} &= I_2 \otimes \begin{bmatrix} 1 & T \\ 0 & 1 \end{bmatrix} \\ Q &= \sigma_w^2 I_2 \otimes \begin{bmatrix} T^3/3 & T^2/2 \\ T^2/2 & T \end{bmatrix} \end{aligned} \tag{31}$$

where $\otimes$ is the Kronecker product, I_n denotes the identity matrix of n dimensions, $T = 1$ s is the sampling period, and $\sigma_w^2 = g^2/T$, where $g = 9.82\,\mathrm{m/s^2}$, is the process noise variance.

A receiver is located at the origin of a Cartesian two-dimensional plane and generates measurements from four co-located antennas. Each antenna operates either as a surveillance or as a reference antenna. The antennas are configured in the directions $\theta \in \Theta$, where $\Theta = \{45°, 135°, 225°, 315°\}$ relative north to cover all directions around the receiver. To handle measurements from multiple transmitters we define a sensor $\boldsymbol{s} = [x^{\mathrm{tx}}, \gamma]$ as one bistatic pair with a transmitter x^{tx} along with one reference antenna directed at θ_r and one surveillance antenna at θ_s as the configuration $\gamma = [\theta_r, \theta_s]$, where $\theta_r, \theta_s \in \Theta$ and $\theta_r \neq \theta_s$. The measurements are distributed as described in (16) where the standard deviation of the range noise is $\sigma_r = 1\,000$ m and range rate noise is $\sigma_{\dot{r}} = 2$ m/s. The probability of the sensor for detecting a target

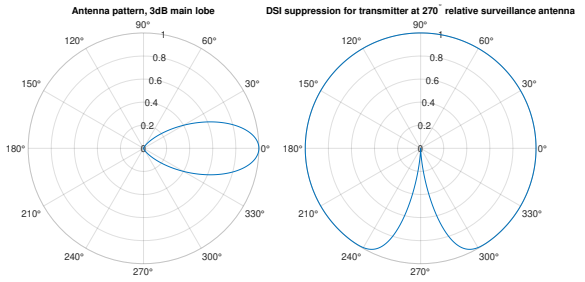

Fig. 2: Left: Antenna pattern as a function of target angle relative the antenna. Right: Attenuation of direct signal from transmitter.

TABLE I: PMBM filter parameters

Parameter	Symbol	Value
Time step	T	1 s
Maximum global hypotheses	$N_h^{\max}$	200
Poisson prune threshold	τ_p	10^{-5}
Global hypothesis prune threshold	τ_g	10^{-5}
Existence threshold	τ_r	0.1
Existing target gate threshold	τ_{g}^e	20
Poisson gate threshold	τ_{g}^e	15
Target extraction threshold	τ_r^t	0.4

is computed using (17)-(18) and is capped at $p_{\text{D}}^{\max} = 0.7$. The SNR loss terms are illustrated in Fig. 2 and set to

$$\begin{aligned} L_A(x_k; x^{\text{tx}}, \theta) &= \cos(0.47\phi_k^A)^{30} \\ L_{\text{DSI}}(x_k; x^{\text{tx}}) &= 1 - \text{sinc}(\phi_k^{\text{DSI}})^{10} \\ \phi_k^A &= \arctan\left(\frac{(p_k^x - p_x^{\text{tx}})\sin\theta_s + (p_k^y - p_y^{\text{tx}})\cos\theta_s}{(p_k^x - p_x^{\text{tx}})\cos\theta_s - (p_k^y - p_y^{\text{tx}})\sin\theta_s}\right) \\ \phi_k^{\text{DSI}} &= \arctan\left(\frac{p_k^x \sin\theta_{\text{tx}} + p_k^y \cos\theta_{\text{tx}}}{p_k^x \cos\theta_{\text{tx}} - p_k^y \sin\theta_{\text{tx}}}\right) \end{aligned} \quad (32)$$

where θ_{tx} is the direction to the transmitter from the receiver. The false alarm intensity is set to $\lambda^{\text{FA}}(z) = 10^{-8}$.

The birth PPP is a Gaussian mixture with components evenly distributed on the surveillance area boundary (see Sec. III-B). The separation between components is $d_b = 5\,000$ m. Each component has mean $x_k^b = [p_k^{x,b}, p_k^{y,b}, 0, 0]^T$ and covariance $P_k^b = \text{diag}([5000^2, 5000^2, 250^2, 250^2])$. New targets arrive with rate $w^b = 1/30$ s, *i.e.* two per minute.

Targets are estimated with a PMBM filter (see Sec. II-B) together with proposed PBR adaptations (see Sec. III-C). To reduce the computational complexity, Bernoulli component recycling is applied [16]. Components with existence lower than a threshold τ_r are recycled into the undetected target intensity. Extraction of estimated targets is performed by taking the belonging Bernoulli components, with probability of existence above a threshold τ_r^t, to the global hypothesis with highest weight [5]. Filter parameters are listed in Table I. In the evaluations we refer the approach with a Gaussian mixture state density as *Mixture* and the standard approach as *Single*.

A. Simulated scenario

The simulated scenario is a multi-target scenario that involves simulated measurements of four sensors. The purpose of this scenario is to evaluate tracking performance according two two criteria: number of targets and false measurements rate. The scenario lasts for 100 time steps where measurements and ground truth are simulated for each time step. Simulated targets enter the surveillance area on the boundary and never die. The probability of detection on he boundary is $p_{\text{D}}^{\min} = 0.3$ in at least $N_S^{\min} = 2$ sensors. The receiver is limited to $[r^{\min}, r^{\max}] = [20\,\text{km}, 350\,\text{km}]$ and $[\dot{r}^{\min}, \dot{r}^{\max}] = [-600\,\text{m/s}, 600\,\text{m/s}]$, respectively. Simulated measurement noise is zero-mean Gaussian distributed with covariance $\text{diag}([1000^2, 1^2])$. The design parameter L_D in (17) is set so the probability of detection is 0.3 at maximum bistatic range $r^{\max}$ for each sensor. Fig. 3 illustrates the scenario geometry. Simulation parameters are listed in Table II.

Number of targets: Target arrival is simulated as a Poisson process at multiple rates, λ_{sim}^T. Target birth is uniformly distributed over the surveillance area boundary. Targets move with constant velocity directed inwards the center of the surveillance area. The speed is uniform in the interval [280 km/h, 1 000 km/h], to represent multiple types of aircraft.

False measurements: False sensor measurements are simulated as a Poisson process at multiple rates, $\lambda_{\text{sim}}^{\text{FA}}$, per scan and sensor. False measurements are uniformly distributed according to Sec. III-A.

The GOSPA RMS error and its components are illustrated in Fig. 4. The results are averaged over 100 Monte Carlo runs for all configurations of the parameters λ_{sim}^T and $\lambda_{\text{sim}}^{\text{FA}}$.

TABLE II: Simulation parameters

Parameter	Symbol	Value
Scenario length	T_{sim}	100 s
Monte Carlo runs	N_{mc}	100
Target arrival rates	λ_{sim}^T	$[1, 5, 10]\,\text{min}^{-1}$
False measurements rates	$\lambda_{\text{sim}}^{\text{FA}}$	$[0.1, 1, 10, 15, 20]\,\text{s}^{-1}$

The mixture approach performs better than the single approach when we compare the RMS GOSPA error for all configurations. The difference is smaller at lower λ_{sim}^T but increases at larger λ_{sim}^T. The localization error is smaller for the single approach but not for false and missed targets. The biggest difference is for missed targets. The mixture approach tends to miss fewer targets. The difference in false target error is smaller but the mixture approach tends to report fewer false targets. This indicates that the mixture approach helps the filter to report a correct number of targets.

B. Real scenario

The scenario consists of two sub-scenarios: maneuvering target and area surveillance. In the first, we investigate how the filter performs with a maneuvering target. Multiple targets are present, but in the evaluation we are just interested in the single target. In the second scenario we investigate filter performance in an aerial surveillance scenario with multiple targets. At the boundary, the probability of detection is $p_{\text{D}}^{\min} = 0.7$ in at least $N_S^{\min} = 2$ sensors. Data is collected using a measurement system with four coherent channels. The design parameter K in (17) is set so the probability of detection is 0.5 at maximum

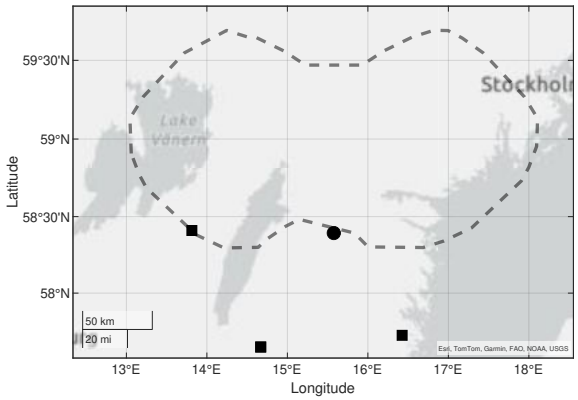

Fig. 3: Geometry of the simulated scenario where the receiver is illustrated by a filled circle and transmitters as filled squares. The boundary of the surveillance area is illustrated by the dashed line.

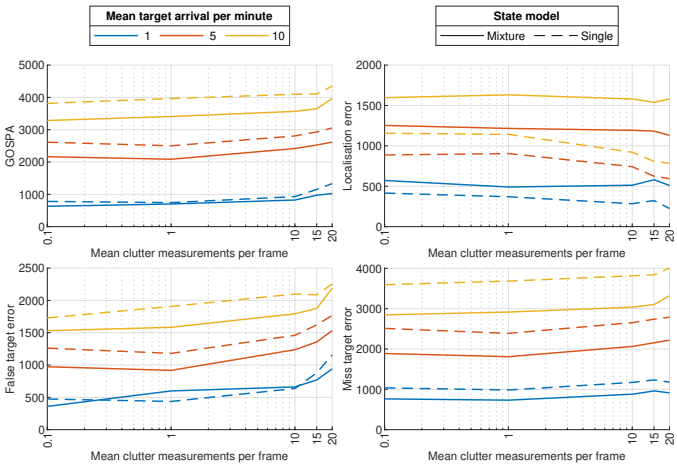

Fig. 4: Results averaged over 100 Monte Carlo runs as a function of simulated false measurement rate ($\lambda^{\text{FA}}_{\text{sim}}$) for three values of simulated targets arrival rate (λ^{T}_{sim}).

bistatic range $r^{\max}$ for each sensor. Bistatic measurements are extracted using a cell-averaging constant false alarm rate (CA-CFAR) detector [13] with parameter $P_{\text{FA}} = 10^{-6}$.

Ground truth is extracted from ADS-B and from an onboard inertial navigation system (INS) supported by global navigation satellite system (GNSS) on the cooperative target.

Scenario 1: Area surveillance: Resembles the simulated scenario in the sense that multiple targets are present in the surveillance area, see Fig. 5. It lasts for 300 time steps, with a total of seven targets, of which four are present from the start. Four transmitters are selected to cover the area to the east of the receiver. The receiver is limited to $[r^{\min}, r^{\max}] = [50\,\text{km}, 350\,\text{km}]$. Targets present from start are added to the undetected targets intensity prior as Gaussian components with weight $w = 1/4$. Each component has mean $x_{0|0} = [p^x_{\text{ADS-B}}, p^y_{\text{ADS-B}}, v^x_{\text{ADS-B}}, v^y_{\text{ADS-B}}]^T$ and covariance $P_{0|0} = \text{diag}([1000^2, 1000^2, 50^2, 50^2])$ using reported data from ADS-B.

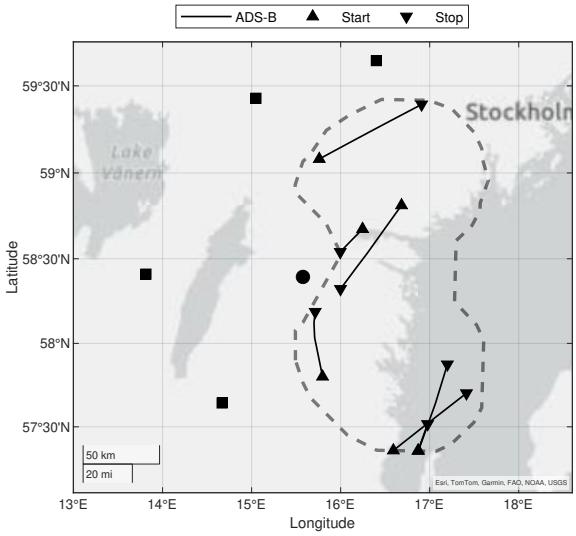

Fig. 5: The area surveillance scenario. The recording lasts for five minutes and four transmitters are selected, illustrated with filled squares. The surveillance area boundary is illustrated by a dashed line.

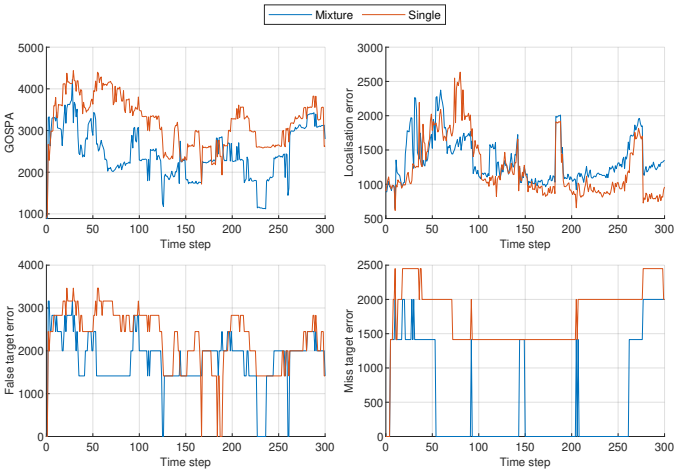

Fig. 6: GOSPA and its components as a function of time for the mixture and single approaches in the area surveillance scenario.

In Fig. 6 we see that the mixture approach results in lower GOSPA RMS error explained by a smaller number of missed targets and false targets. The localization error is lower with the single approach, but with a higher number of missed and false targets. For an aerial surveillance application a large number of false and missed targets is not favorable, which supports the mixture approach.

Scenario 2: Maneuvering target: This scenario focuses on a cooperative target but other targets are present, see Fig. 7. The scenario lasts for 800 s and no target is present from the start. The cooperative target flies at constant altitude and enters the surveillance area from the west 45 s into the scenario. In the area it flies straight lines combined with some maneuvers

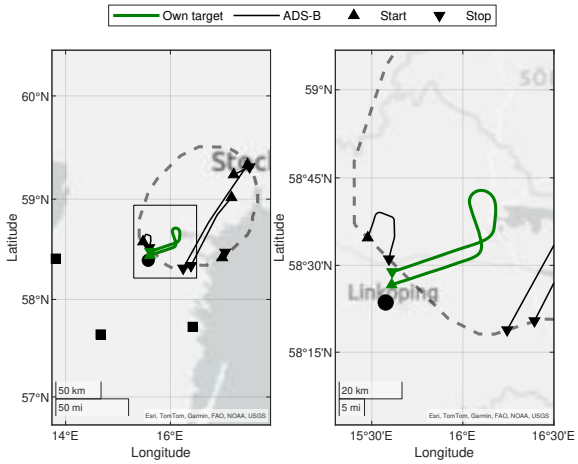

Fig. 7: The maneuvering target scenario. Left: Overview of the scenario with three transmitters, surveillance area boundary and ground truth targets. Right: Zoomed-in view where the trajectory of the cooperative target is more prominent.

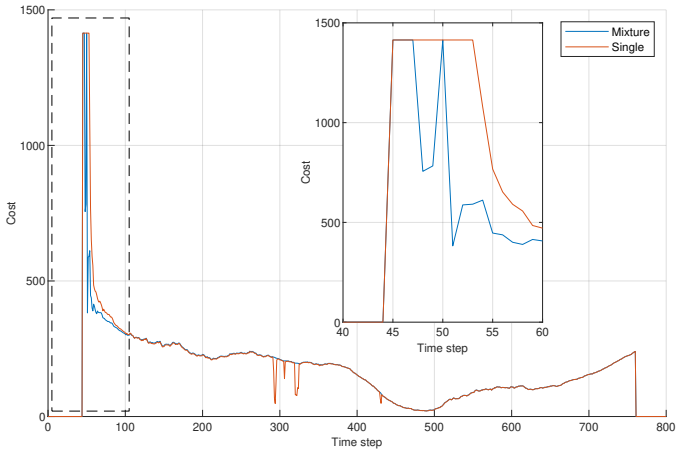

Fig. 8: Sum of localization error and missed target GOSPA sub-components against time for both approaches in Scenario 2. The inset plot is a zoomed-in view of the area marked with a dashed line.

before it exits at time 760 s. Three transmitters are selected. The receiver is limited to $[r^{\min}, r^{\max}] = [20\,\text{km}, 350\,\text{km}]$.

Fig. 8 shows the sum of the localization error and missed target GOSPA sub-components as a function of time for the single target only. Both approaches perform almost equally over the entire scenario. In the inset plot in Fig. 8 we see that a true target is reported earlier with the mixture approach. The filter handles the target maneuvers equally for both approaches. The noticeable jumps for the single approach around time step 300 in the large plot is due to a false target that is associated to the ground truth target.

To summarize, the results show that the proposed methods to handle PBR measurements result in better tracking performance in terms of GOSPA compared to the standard PMBM filter implementation.

V. Conclusion

In this paper we have presented an approach to handle PBR in a multi-target tracking context using the PMBM filter. It is proposed that a Gaussian mixture is used to represent the target state density. We also present modeling of the PBR sensor to exploit the PBR properties during target birth and provide a state dependent probability of detection. From a standard PMBM implementation we present required modifications and additions. With our approach, better results are obtained compared to the standard implementation, which is verified through experiments. The results are promising and are valuable for future work.

Acknowledgments

This paper was funded by the Swedish strategic research center Security Link through the project Advanced Data Fusion Methods in Multi-Static and Multi-Channel Passive Radar (DFMR). The work has also been supported by research projects at the Swedish Defence Research Agency (FOI), which are funded by the Swedish Armed Forces R&D programme.

References

[1] S. Blackman and R. Popoli. Modern tracking systems. *Artech House*, 1, 1999.

[2] D. Crouse. Basic tracking using nonlinear 3D monostatic and bistatic measurements. *IEEE Trans. Aerosp. Electron. Syst.*, 29(8), 2014.

[3] M. Daun and W. Koch. Multistatic target tracking for non-cooperative illumination by DAB/DVB-T. In *Proc. 2008 IEEE Radar Conf.*, 2008.

[4] D. Fränken and O. Zeeb. Real-time creation of a target situation picture with the Hensoldt passive radar system. In *Proc. 21th IEEE Int. Conf. Inform. Fusion*, Cambridge, UK, July 10–13 2018.

[5] A. F. Garciá-Fernández, J. L. Williams, K. Granström, and L. Svensson. Poisson multi-Bernoulli mixture filter: Direct derivation and implementation. *IEEE Trans. Aerosp. Electron. Syst.*, 54(4), 2018.

[6] H. Griffiths and C. J. Baker. *An Introduction to Passive Radar*. Artech House, 2017.

[7] G. Hendeby and R. Karlsson. Gaussian mixture PHD filtering with variable probability of detection. In *Proc. 17th IEEE Int. Conf. Inform. Fusion*, Salamanca, Spain, July 7–10 2014.

[8] S. Herman and P. Moulin. A particle filtering approach to FM-band passive radar tracking and automatic target recognition. In *Proc. IEEE Aerospace Conference*, 2002.

[9] R. Mahler. *Statistical Multisource-Multitarget Information Fusion*. Artech House, 2007.

[10] R. Mahler. Approximate multisensor CPHD and PHD filters. In *Proc. 13th IEEE Int. Conf. Inform. Fusion*, Edinburgh, UK, July 26–29 2010.

[11] M. Malanowski, K. Kulpa, and R. Suchozebrski. Two-stage tracking algorithm for passive radar. In *Proc. 12th IEEE Int. Conf. Inform. Fusion*, Seattle, July 6–9 2009.

[12] A. S. Rahmathullah, A. F. Garciá-Fernández, and L. Svensson. Generalized optimal sub-pattern assignment metric. In *Proc. 20th IEEE Int. Conf. Inform. Fusion*, Xi'an, China, July 10–17 2017.

[13] M. A. Richards, J. A. Scheer, and W. A. Holm, editors. *Principles of Modern Radar: Basic principles*. IET, 2010.

[14] S. Subedi, Y. D. Zhang, M. G. Amin, and B. Himed. Group sparsity based multi-target tracking in passive multi-static radar systems using doppler-only measurements. *IEEE Trans. Signal Process.*, 64(14), 2016.

[15] M. Tobias and A. D. Lanterman. Probability hypothesis density-based multitarget tracking with bistatic range and doppler observations. *IEE Proc. Radar Sonar Navig*, 152, June 2005.

[16] J. L. Williams. Hybrid Poisson and multi-Bernoulli filters. In *Proc. 15th IEEE Int. Conf. Inform. Fusion*, Singapore, July 9–12 2012.

[17] J. L. Williams. Marginal multi-Bernoulli filters: RFS derivation of MHT, JIPDA, and association-based MeMBer. *IEEE Trans. Aerosp. Electron. Syst.*, 51(3), 2015.